



Electrochemical capacitance-voltage profiling of nonuniformly doped GaAs heterostructures with SQWs and MQWs for LED applications

George YAKOVLEV^{1,*} , Vasily ZUBKOV¹ , Anna SOLOMNIKOVA¹ ,
Oleg DEREVIANKO² 

¹St. Petersburg State Electrotechnical University (LETI), St. Petersburg, Russia

²Peter the Great St. Petersburg Polytechnic University, St. Petersburg, Russia

Received: 17.03.2018

Accepted/Published Online: 09.05.2018

Final Version: 15.08.2018

Abstract: Light-emitting heterostructures with single and multiple GaAs/InGaAs quantum wells have been investigated by means of electrochemical capacitance-voltage (ECV) profiling. Capacitance-voltage characteristics were measured; concentration profiles of free charge carriers over the heterostructure depth as well as the intensity of quantum well filling by charge carriers were obtained. In heterostructures with a single quantum well (QW) we considered limitations of capacitance techniques for undoped QW profiling, which is situated near the metallurgical border of the $p-n$ -junction. We made a detailed consideration of phenomena related to Debye smearing and we developed and analyzed the dependence of the space charge region width on the doping. Special attention was paid to investigation of the “blind” area. This was inspired by the practical problem from capacitance spectroscopy of semiconductors, when the researcher poses the task of obtaining a free charge carrier depth distribution profile as deep as possible in the space charge region, i.e. where the intensity of the electric field is maximum. Generally, the active QW of a LED heterostructure is placed deep in the space charge region, so reaching these regions is extremely important for practical problems. We present an evolution of capacitance-voltage characteristics during ECV profiling of nonuniformly doped $p-n$ -heterostructures. For a heterostructure with multiple quantum wells we registered a response from 6 QWs.

Key words: Electrochemical capacitance-voltage profiling, heterostructure, light-emitting diodes, quantum well, quantum dot, capacitance-voltage profiling, nonuniform doping

1. Introduction

Semiconductor heterostructures with single quantum wells (SQWs) and multiple quantum wells (MQWs) are successfully used for nano- and optoelectronics devices such as light-emitting diodes, lasers, and photodetectors [1–6]. Despite the long history of heterostructure development, this research area still possess some unsolved problems, while these issues are still of great scientific interest. A special feature of these heterostructures is the sharply nonuniform distribution of doping impurity, used for improvement of device characteristics. Quantum wells create a well-pronounced free charge carrier (FCC) distribution profile regardless of the impurity distribution over the structure. This profile has sharp enrichment peaks at the potential drop area, even despite the fact that QWs and spacer layers generally are not being doped in order to decrease the defect density and thus depress the probability of nonradiating transitions [7]. The requirements concerning impurity composition and its distribution over the end devices are constantly increased, so the structures become more and more

*Correspondence: gy@etu.ru

complicated [8]. The processes used for structure fabrication are often very complicated, and the results are greatly affected by initial material purity and technological routes of layer fabrication [9–13]. Thus, the impurity and FCC distribution control techniques are facing increasing demand both at the laboratory development stage and at various technological stages of end device production.

The electrochemical capacitance-voltage (ECV) profiling technique allows one to obtain information about both impurity distribution and FCC concentration [14]. Whereas the ECV measurements of uniformly doped semiconductor structures are well investigated and are considered as routine tasks, the measurement of modern multilayer light-emitting heterostructures with non-uniform impurity profiles appears to be a rather difficult task [15]. Furthermore, there are some difficulties concerning the interpretation of experimental results for capacitance-voltage characteristic measurements of light-emitting diodes (LEDs) with QWs. The reasons are the following: deviation from the quasistatic regime, space charge region (SCR) expansion both to n - and p -regions, and deep center properties of the examined energy level, which are expressed in capacity response delays [16].

The main purposes of the present work were to investigate special aspects of FCC depth distribution in modern GaAs LED heterostructures and to analyze the ECV technique resolution in the case of nonuniform doping profile measurements. We also discuss some features of capacitance-voltage profiling result interpretation concerning heterostructures with SQWs and MQWs, particularly the “blind” area effect.

2. The investigated samples

We examined a set of 5 GaAs heterostructures intended for fabrication of IR light-emitting diodes. Layer sequences of the samples are presented in Figure 1. Samples 1–4 (Figure 1a) are heterostructures with $\text{In}_x\text{Ga}_{1-x}\text{As}/\text{GaAs}$ QWs, grown by MOCVD at the Ferdinand-Braun-Institut (Berlin, Germany). The heterostructures have nonuniform doping of n - and p -layers with concentration decrease toward the quantum well. The samples differ from one another by doping level and layer width. Doping levels of the p -areas varied from $1 \times 10^{18} \text{ cm}^{-3}$ to $1 \times 10^{17} \text{ cm}^{-3}$, while for n -areas the doping level range was from 2×10^{18} to $3 \times 10^{17} \text{ cm}^{-3}$. QW width was 7 nm and indium content varied from 0.27 to 0.35.

| | | |
|--|------------|-------|
| p-GaAs | 100-300 nm | } x10 |
| p-GaAs | 100-300 nm | |
| p-GaAs | 100-200 nm | |
| p-GaAs undoped | 100 nm | |
| GaAs undoped | 13 nm | |
| InGaAs | 7nm | |
| GaAs undoped | 13 nm | |
| n-GaAs undoped | 100 nm | |
| n-GaAs | 200-500 nm | |
| n-Al _{0.25} Ga _{0.75} As | 100 nm | |
| n-Al _{0.25} Ga _{1-0.75} As | 40 nm | |
| n-GaAs | 100 nm | |
| p ⁺ -GaAs | 50 nm | |
| p-Al _{0.2} Ga _{0.8} As | 150 nm | |
| p-Al _{0.4} Ga _{0.6} As | 1500 nm | |
| i-GaAs | 50nm | |
| In _{0.15} Ga _{0.85} As | 6 nm | |
| InAs QD | 2.7 ML | |
| p-GaAs | 50 nm | |
| n-Al _{0.4} Ga _{0.6} As | 1500 nm | |
| n ⁺ -GaAs | 300 nm | |
| n ⁺ -GaAs substrate | | |

Figure 1. Layer sequence of the examined samples: a) heterostructures with $\text{In}_x\text{Ga}_{1-x}\text{As}/\text{GaAs}$ QWs (samples Nos. 1-4); b) heterostructure with multiple QWs and QDs (sample No. 5).

The layer sequence of sample No. 5, which contains MQWs and quantum dots (QDs), is presented in Figure 1b. This heterostructure was grown by MBE technique [17]. The p^+ -GaAs cap layer of 50 nm in width

was nonuniformly doped with concentration decreasing into the structure's depth from $3 \times 10^{19} \text{ cm}^{-3}$ to $5 \times 10^{18} \text{ cm}^{-3}$. Layers $p\text{-Al}_{0.2}\text{Ga}_{0.8}\text{As}$ and $p\text{-Al}_{0.4}\text{Ga}_{0.6}\text{As}$ were doped up to $5 \times 10^{18} \text{ cm}^{-3}$. The undoped GaAs spacer layer, which divides ten layers of QDs and QWs, has concentration of 10^{14} cm^{-3} , which is typical for MBE, and acquires p -type conductivity. After ten QW and QD layers, there is a p -GaAs layer of 50 nm in width with $5 \times 10^{17} \text{ cm}^{-3}$ doping level. Layer $n\text{-Al}_{0.4}\text{Ga}_{0.6}\text{As}$ was Sb-doped up to $4 \times 10^{18} \text{ cm}^{-3}$.

3. ECV measurement technique

The classical capacitance-voltage (C-V) profiling technique is widely used for characterization of semiconductor materials and structures. In order to obtain the FCC concentration distribution, one has to measure its capacitance in an available bias range. The ECV is the improvement of the classical C-V measurement technique. The conventional C-V technique is performed by monitoring the barrier capacitance of the sample during the sweeping of the applied bias (the sample needs a fabricated metal Schottky contact). However, in many semiconductor structures like LEDs, which have heavily doped layers on the top, the implementation of this technique will result in limitation for the apparent FCC depth profile (typical profiling depth is less than 50–100 nm). Information about even more deeply located QWs is inaccessible because of the possible breakdown of the structure at high applied voltages. In the ECV technique, the liquid electrolyte is used both as a rectifying contact and as an etchant for controlled dissolution of the semiconductor. It helps to overcome the abovementioned limitations and to obtain full information about the FCC distribution in the sample [18]. Thus, the typical ECV measurement process consists of alternating CV measurements and electrochemical etching [19]. In the ECV technique, like in plain C-V, the FCC concentration is calculated as the derivative of the measured dependence of capacitance vs. bias [20]:

$$n(x_d) = -\frac{C^3}{q\varepsilon\varepsilon_0S^2} \left(\frac{dC}{dV}\right)^{-1}, \quad (1)$$

where q is the elementary charge, ε is the dielectric permeability of the investigated material, ε_0 is the electrical constant, C is the capacitance, V is the applied bias, and S is the area of electrolyte-semiconductor contact. The location of the space charge region edge (or coordinate where the concentration is measured) is defined as

$$x_d = \frac{\varepsilon\varepsilon_0S^2}{C}. \quad (2)$$

In the case of ECV profiling, dC/dV is usually measured by the two-frequency (modulation) method. Here the small test signals of f_1 and f_2 are imposed sequentially on the specific (constant) DC bias. For common C-V measurements this derivative is calculated by numerical derivation of the measured capacitance-voltage characteristics.

ECV etching depth is determined according to the amount of the removed substance, obtained from electrochemical Faraday law:

$$x_r = \frac{M}{zF\rho S} \int_0^{t_0} i(t)dt, \quad (3)$$

where M is the molar mass, z is the valence number of substance ions (the amount of electrons, which is needed for one molecule to dissolve), F is the Faraday constant, and ρ is the material specific density.

The FCC depth distribution measurements were carried out at room temperature using ECVPro (Nanometrics). Tiron (0.1 M) was used as an electrolyte [21]. The area of the electrolyte rectifying contact was 0.1 cm^2 . Etching current was at the level of 0.5 mA/cm^2 . Etching step was 1 nm. Bias V in ECV measurements was chosen at the linear region of C - V characteristics at Mott–Schottky coordinates ($1/C^2$ vs. V) and was -0.6 V . It should be noted that biases in this work are defined in respect to the reference electrode, and the usage of other electrolytes will result in the change of optimum measurement parameters. The test signal frequency used for capacitance measurements was 138 Hz. In some experiments for determination of capacitance-voltage characteristics we used an Agilent E4980A, which was connected to the electrochemical cell of the ECVPro through a designed relay module [22]. In order to control etching depth and quality we used a Solver NEXT atomic-force microscope.

4. Experimental results and discussion

4.1. Investigation of light-emitting structures with single quantum wells

This part of the work presents FCC depth distribution profiles of GaAs light-emitting heterostructures with SQWs. The obtained concentration profiles are presented in Figures 2–5. Red circles denote hole concentrations and blue ones denote electron concentrations. The results stay within the measurement technique’s accuracy and have good agreement with sample passport data.

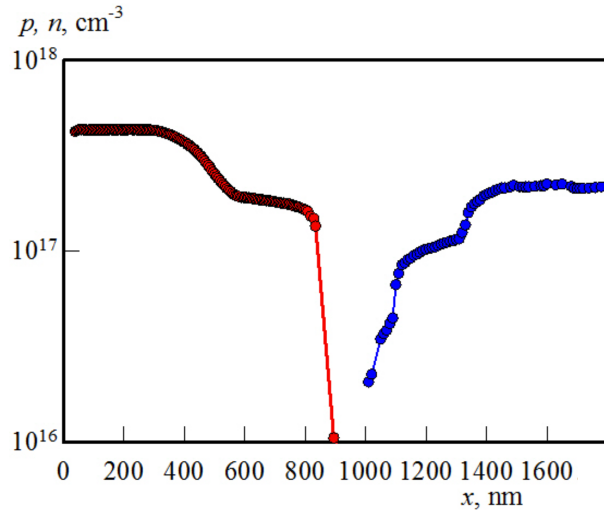


Figure 2. Free charge carrier distribution profiles into the depth of sample No. 1.

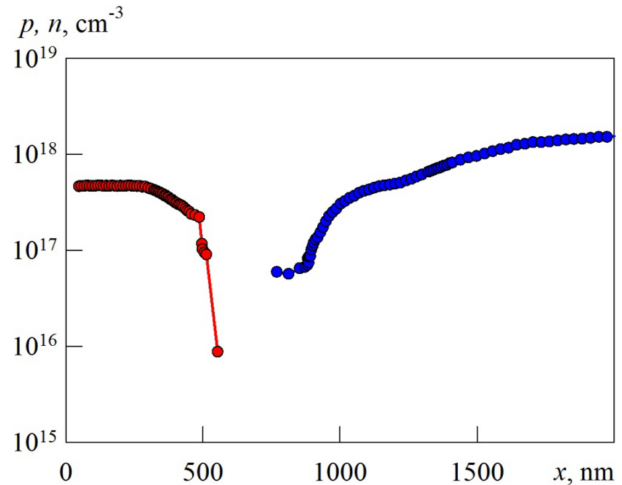


Figure 3. Free charge carriers distribution profiles into the depth of sample No. 2.

It is seen that the concentration profiles possess a “blind” area of about 200 nm, which corresponds to the quantum well and adjacent undoped regions on both sides of it. The reason for this is that to obtain maximum efficiency of charge carrier recombination, the design of this structure was optimized for the presence of a SQW, located directly in the maximum of the p – n -junction electric field. This means that while measuring these structures by capacitance techniques, we cannot register a response from an area that corresponds to a quantum well. The apparent advantage of the ECV technique is the possibility of profiling in the etching mode; however, even in this case we do not see a response from the QW at the concentration profile. This can be explained as follows: during the etching process, due to nonuniform doping of surface layers, the electrolyte/semiconductor interface shifts to the area with over decreasing concentration. This is accompanied by a nonlinear increase of

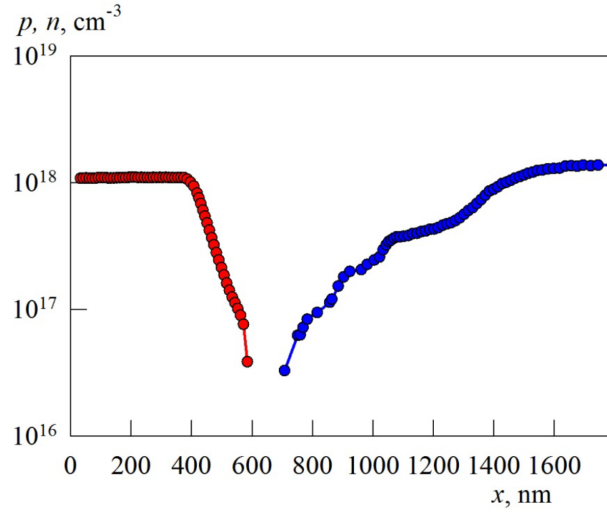


Figure 4. Free charge carriers distribution profiles into the depth of sample No. 3.

space charge region width, on which edge we measure the apparent FCC concentration. Our previously obtained experimental relation between SCR width and doping level of the profiling layer is presented in Figure 6. It is also important to take into account QW depletion regions, which are located at both sides of it.

Let us mention the principle difference between impurity and FCC distributions: the latter redistribute under the impact of alternating voltage, which is applied in C-V measurements. Thus, they form a smearing profile, which is characterized by Debye screening length. Consequently, by measuring a differential capacitance, one may define the “apparent” concentration profile of free charge carriers. Technically, this profile does not match either the true FCC concentration profile (obtained for equilibrium condition without external bias) or the impurity distribution profile [23]. Using iteration calculations [24], one can reconstruct the true FCC distribution profile; however, it is rarely done due to mathematical difficulty.

As was mentioned above, as free charge carriers diffuse into the adjacent areas (including the depletion area), they will not show an impurity distribution for an area of sharp doping profile. In these areas one can observe “profile smearing” for some Debye lengths, which eventually determines the fundamental resolution of the implemented measurement technique (Figure 7). The analysis shows that if the doping level step takes place within one Debye screening length, then the apparent and true FCC concentration profiles will be in good agreement with each other, but noticeably different from the impurity profile [22].

This effect is most pronounced in the structures with sharply nonuniform doping profiles, such as in HEMT structures [25,26] or in structures with delta-doped layers, where the doping area itself is just some Debye lengths. At this concentration peak the amplitude appears to be underestimated, and the peak itself is broadened and smeared along the coordinates. The sharper the doping profile, the bigger the difference is between observed FCC concentration and impurity concentration. This difference is characterized by Debye screening length:

$$L_D = \sqrt{\frac{kT\varepsilon\varepsilon_0}{q^2(p+n)}}. \quad (4)$$

The presence of Debye length results in inability of profiling for distances nearer than 2–3 L_D from surface area.

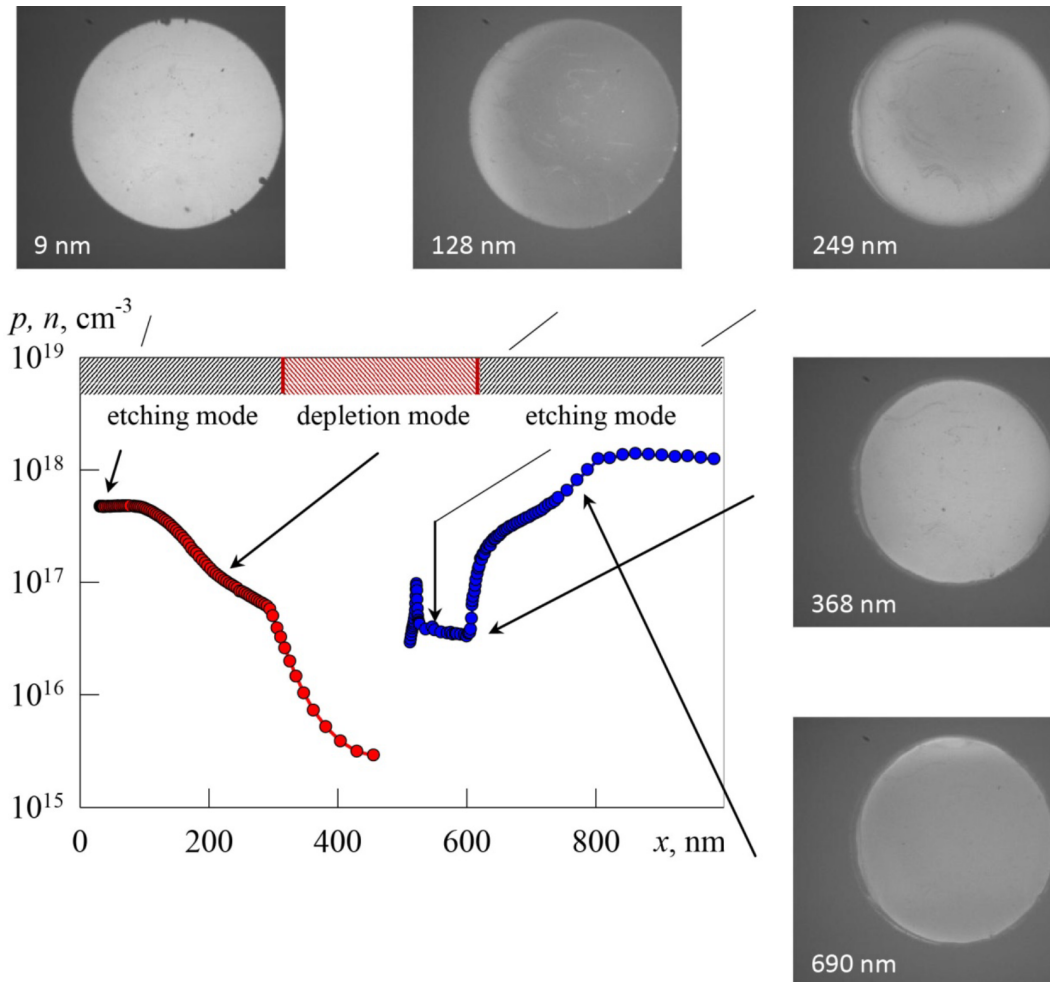


Figure 5. Free charge carriers distribution profiles into the depth of sample No. 4.

For semiconductors, which are doped up to degeneracy, coordinate resolution is limited by Debye length for Thomas–Fermi model approximation [27], which is denoted by the following expression:

$$L_{TF} = \left(\frac{\pi}{3(p+n)} \right)^{1/6} \sqrt{\frac{\pi\epsilon\epsilon_0\hbar^2}{q^2m^*}}. \quad (5)$$

For semiconductors with quantum-sized areas, for example with δ -layers of QWs, the Debye length as a degree of concentration profile smearing is defined using the squared absolute value of ground state wave function $|\Psi(x)|^2$ [27]:

$$L_\delta = 2\sqrt{\frac{7}{5}} \left(\frac{4\epsilon\epsilon_0\hbar^2}{9q^2N_{2D}m^*} \right)^{1/3}, \quad (6)$$

where $N_{2D} \sim |\Psi(x)|^2$ is the two-dimensional impurity concentration. This expression shows that resolution for measurement of materials with high effective masses is higher than that for materials with lower ones. For example, the resolution for p -GaAs measurement is higher than that for n -GaAs.

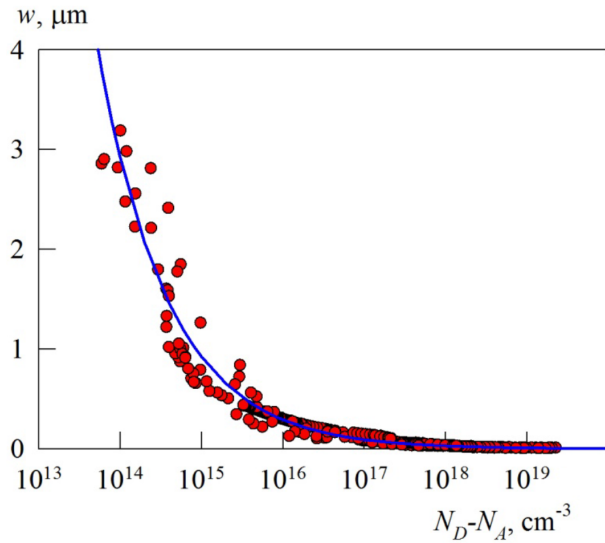


Figure 6. The experimental relation between SCR width and doping level of the profiling layer.

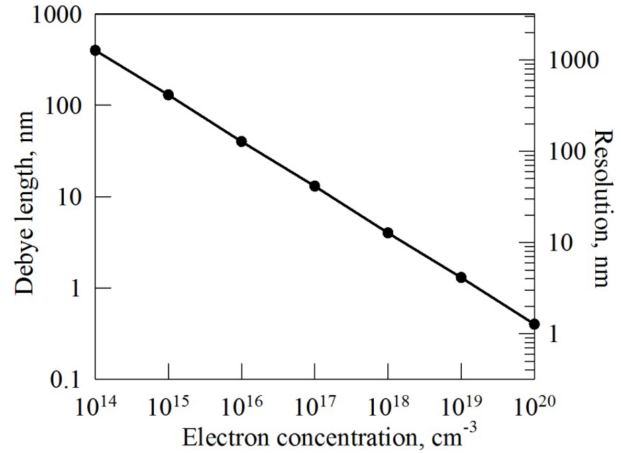


Figure 7. Relation between the Debye length, ECV technique coordinate resolution, and charge carrier concentration in a semiconductor.

The model and calculation formulas used for recalculation of measured C-V characteristics into the FCC depth distribution profile are also applicable for asymmetric $p-n$ -junctions, i.e. p^+n - or n^+p - junctions. When the doping level of the heavily doped area is 100 or more times higher than that for the adjacent area, one can neglect the profile smearing towards the heavily doped area.

In our case, doping of samples 1–4 is nonuniform with 3 orders of concentration drop. The Debye smearing effects and change of conductivity type are added to the limitations due to the sharp SCR width increase at the vicinity of the QW. Measurements in this area are accompanied by high noise level (due to dissipation factor increase up to ~ 0.4); we guess it to be unreliable.

The estimations show that the stepwise doping profile in Figures 2–5 cannot be resolved by coordinates with accuracy better than $2-3 L_D$, and the Debye length L_D is defined by the concentration from the heavily doped side. Thus, despite the shift of Schottky contact due to material etching, the QW always turns out to be inside the SCR: at the beginning of the measurement the SCR edge under the Schottky contact does not reach the QW location. Furthermore, in the course of intensive enlarging of the SCR due to doping level drop, the merger of two depletion areas (under the Schottky barrier and the SCR around the QW) takes place. It should be noted that SCR width of a $p-n$ -junction cannot be equal to zero, but it may have dimensions of some nanometers at high doping levels adjacent to QW p - and n -areas. Then, according to the Gauss theorem, the SCR width at which the required charge amount for external bias screening is collected will be extremely low. At small bias increment ΔV theoretically we will be able to carry out QW profiling with adequate resolution.

In a number of cases, the change in the experimental parameters due to errors associated with the illumination region led to an insignificant increase in the scatter of the measured concentration value upon transition to n -type conductivity layers (illumination is mandatory for ECV etching of n -type layers). This is illustrated in Figure 5 by comparing the surface photos of the etching crater bottom of sample No. 4 as the experiment is carried out. The captions on the photos correspond to the coordinates in the depth of the structure (etching depth).

The measurements of LED structures with SQWs allow one to estimate the size of the “blind” area: for

any attempts of profiling the active region of a semiconductor with space charge region, we could not register the concentration of charge carriers in a certain region, which corresponds to the maximum of the electric field due to the fact that an immediate merging of SCRs occurs. One would think that with a free choice of ECV profiling depth, it is possible to profile all the layers within the active region, but this is impossible because of the presence of a “blind” area that determines the minimum increment in the SCR width in response to the minimum possible increment of externally applied bias. Thus, at a concentration of $\sim 10^{14} \text{ cm}^{-3}$ and an increment of the external applied bias ΔV_{min} of 1 mV, the corresponding increment value of the SCR will be about 200 nm. We could suggest that “blind” area size is proportional to k/N , where k is a normalization constant and N is semiconductor doping level. In the other cases, when a QW appears to be shifted from the electric field maximum at the metallurgic border area (as happened with sample No. 4), it becomes possible to perform QW area profiling (insert in Figure 5). An additional feature of the ECV technique in contrast to classical C-V profiling is the permanent change of the C-V characteristic slope due to the gradual shift of the interface during the sample’s in-depth profiling process. Sometimes it allows observing the inversion of $1/C^2$ dependence (Figure 8, sample No. 4); at this cut-off bias will change when passing from layer to layer. The obtained C-V characteristics can be divided into 3 types:

- I. Etching at 1–104 nm depth, no features are seen in the plots;
- II. Etching at 128–207 nm depth, we observe a maximum at the C-V characteristic when SCR edge is reaching the QW area;
- III. Further etching at 228–974 nm depth, where a transition to n -type conductivity takes place, which is firstly accompanied by a sharp increase of capacitance (when profiling QW area and metallurgic contact) and then its gradual relaxation to the normal value.

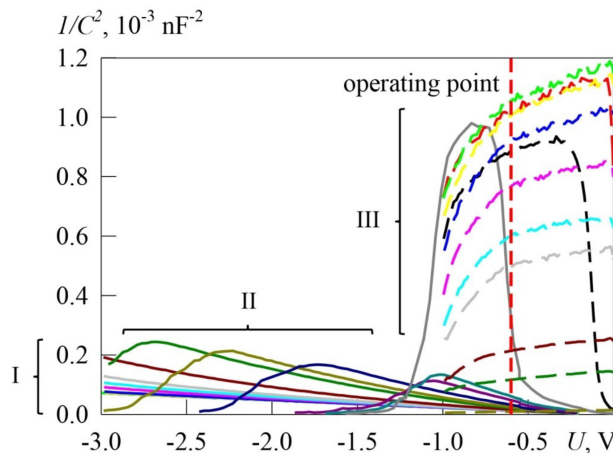


Figure 8. Evolution of C-V characteristics during electrochemical capacitance-voltage profiling of sample No. 4.

The measured capacitance is slowly decreasing during n -area profiling. This could be explained in the following way: etching still takes place in the p -area, while the SCR edge is already located at the n -area.

4.2. Investigation of light-emitting structure with MQWs

In order to confirm the hypothesis that the absence of response from a SQW at capacitance measurements is driven by its location in the maximum of the $p-n$ -junction electric field, we investigated a structure with MQWs. If our assumption is right, in the case of multiple quantum well profiling we will register a response from at least some of the QWs at concentration profile. Figure 9 presents a measured FCC concentration distribution profile of sample No. 5, which comprises 10 layers of QWs and QDs. The most interesting areas of the concentration profile are presented in large scale in the inserts.

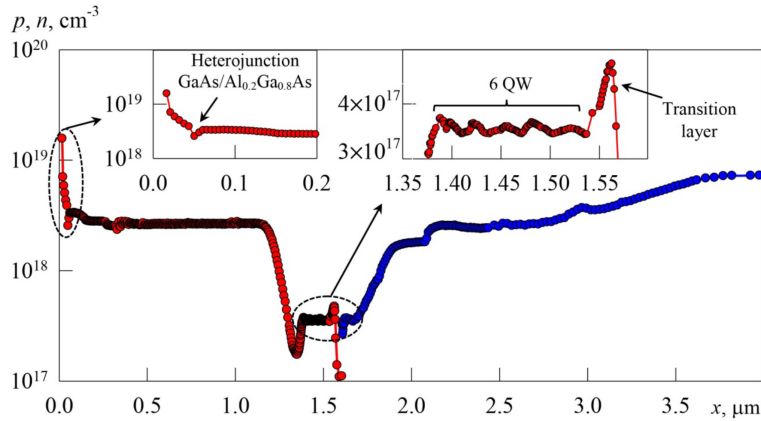


Figure 9. Measured FCC concentration distribution profile of sample No. 5.

As expected, in the case of QWs in isotype claddings, we register a response from multiple QWs. Because of the above-mentioned limitations, we registered six QWs with ~ 50 nm period in the concentration profile, which is in good correlation with sample passport data. It is likely that four other QWs turned out to be inside the “blind” area at a given doping level.

5. Conclusions

Electrochemical capacitance-voltage profiling was used to investigate a set of IR light-emitting heterostructures with SQWs and MQWs based on GaAs/InGaAs. Capacitance-voltage characteristics were measured; concentration profiles of free charge carriers over the heterostructure depth as well as the intensity of quantum well filling by charge carriers were obtained. Limitations and difficulties of capacitance profiling techniques of undoped QWs, located near the metallurgic border of the $p-n$ -junction, were considered. The Debye smearing effects and change of conductivity type are added to the limitations due to the sharp SCR width increase in the vicinity of the QW. Also, at the metallurgic contact the dissipation factor reaches 0.4, causing the drastic increase of losses and the decrease of noise-to-signal ratio. Consequently, it was experimentally shown that even using the ECV technique one could not register the response from the QW located in the maximum of the $p-n$ -junction electric field. The size and features of the “blind” area were investigated in detail. In other cases, when the QW is not in the electric field maximum, or in the case of MQWs, it becomes possible to perform QW profiling. For the heterostructure with multiple quantum wells we have registered a response from 6 QWs, while the other QWs were hidden by the “blind” area.

References

- [1] Nakamura, S.; Senoh, M.; Iwasa, N.; Nagahama, S. I. *Jpn. J. Appl. Phys.* **1995**, *34*, L797-L799.

- [2] Alferov, Z. I. *Phys. Scr. T.* **1996**, *68*, 32-45.
- [3] Firsov, D. A.; Vorobjev, L. E.; Vinnichenko, M. Y.; Balagula, R. M.; Kulagina, M. M.; Vasil'iev, A. P. *Semiconductors* **2015**, *49*, 1425-1429.
- [4] Zhukov, A. E.; Asryan, L. V.; Semenova, L. V.; Zubov, F. I.; Kryzhanovskaya, N. V.; Maximov, M. V. *Semiconductors* **2015**, *49*, 935-938.
- [5] Ramanujam, J.; Verma, A.; González-Díaz, B.; Guerrero-Lemus, R.; Del Cañizo, C.; García-Tabarés, E.; Rey-Stolle, I.; Granek, F.; Korte, L.; Tucci, M. et al. *Prog. Mater. Sci.* **2016**, *82*, 294-404.
- [6] Gökden, S. *Turk. J. Phys.* **2003**, *27*, 205-210.
- [7] Bugge, F.; Zeimer, U.; Sato, M.; Weyers, M.; Tränkle, G. *J. Cryst. Growth* **1998**, *183*, 511-518.
- [8] Memiş, S.; Celtek, O. O.; Bostanci, U.; Tomak, M.; Beşikçi, C. *Turk. J. Phys.* **2006**, *30*, 335-344.
- [9] Kukushkin, S. A.; Mizerov, A. M.; Osipov, A. V.; Redkov, A. V.; Timoshnev, S. N. *Thin Solid Films* **2018**, *646*, 158-162.
- [10] Reznik, R. R.; Kotlyar, K. P.; Soshnikov, I. P.; Kukushkin, S. A.; Osipov, A. V.; Nikitina, E. V.; Cirilin, G. E. *J. Phys. Conf. Ser.* **2017**, *917*, 032014.
- [11] Kryzhanovskaya, N. V.; Moiseev, E. I.; Polubavkina, Y. S.; Maximov, M. V.; Kulagina, M. M.; Troshkov, S. I.; Zadiranov, Y. M.; Lipovskii, A. A.; Baidus, N. V.; Dubinov, A. A. et al. *Opt. Express* **2017**, *25*, 16754-16760.
- [12] Agekyan, V. F.; Borisov, E. V.; Vorobjev, L. E.; Melentyev, G. A.; Nykänen, H.; Riuttanen, L.; Serov, A. Y.; Suihkonen, S.; Svensk, O.; Filisofov, N. G. *Phys. Solid State* **2015**, *57*, 787-793.
- [13] Alexeev, A. N.; Krasovitsky, D. M.; Petrov, S. I.; Chaly, V. P.; Mamaev, V. V.; Sidorov, V. G. *Semiconductors* **2015**, *49*, 92-94.
- [14] Yakovlev, G. E.; Frolov, D. S.; Zubkova, A. V.; Levina, E. E.; Zubkov, V. I.; Solomonov, A. V.; Sterlyadkin, O. K.; Sorokin, S. A. *Semiconductors* **2016**, *50*, 320-325.
- [15] Zubkov, V.; Kucherova, O.; Frolov, D.; Zubkova, A. *Phys. Status Solidi Curr. Top. Solid State Phys.* **2013**, *10*, 342-345.
- [16] Zubkov, V. I. *Diagnostika Poluprovodnikovyh Nanoeterostruktur Metodami Spektroskopii Admittansa*; Elmor: St. Petersburg, Russia, 2007 (in Russian).
- [17] Zubkov, V. I.; Yakovlev, I. N.; Litvinov, V. G.; Ermachihin, A. V.; Kucherova, O. V.; Cherkasova, V. N. *Semiconductors* **2014**, *48*, 917-923.
- [18] Yim, J.; Jones, R.; Yu, K.; Ager, J.; Walukiewicz, W.; Schaff, W.; Wu, J. *Phys Rev B* **2007**, *76*, 1-4.
- [19] Blood, P. *Semicond. Sci. Technol.* **1986**, *1*, 7-27.
- [20] Ambridge, T.; Faktor, M. M. *J. Appl. Electrochem.* **1975**, *5*, 319-328.
- [21] Dorokhin, M. V.; Zaitsev, S. V.; Rykov, A. V.; Zdoroveyshchev, A. V.; Malysheva, E. I.; Danilov, Y. A.; Zubkov, V. I.; Frolov, D. S.; Yakovlev, G. E.; Kudrin, A. V. *Tech. Phys.* **2017**, *62*, 1545-1550.
- [22] Frolov, D. S.; Zubkov, V. I. *Semicond. Sci. Technol.* **2016**, *31*, 125013.
- [23] Johnson, W. C.; Johnson, W. C.; Panousis, P. T. *IEEE T. Electron. Dev.* **1971**, *18*, 965-973.
- [24] Wilson, C. L. *IEEE T. Electron. Dev.* **1980**, *27*, 2262-2267.
- [25] Dudin, A.; Kogan, I.; Schukov, I.; Mironova, M.; Yakovlev, G.; Frolov, D.; Zubkov, V.; Glinskii, G. In *Proceedings of the 2017 11th International Workshop on the Electromagnetic Compatibility of Integrated Circuits*; EMCCompo: St. Petersburg, Russian Federation, 2017, pp. 108-111.
- [26] Yakovlev, G.; Frolov, D.; Zubkov, V. *J. Phys. Conf. Series*, **2016**, *690*, 012015.
- [27] Schubert, E. F.; Kuo, J. M.; Kopf, R. F. *J. Electron. Mater.* **1990**, *19*, 521-531.